

# Structure, bonding, and hardness of CrB<sub>4</sub>: a superhard material?

Haiyang Niu<sup>1</sup>, Jiaqi Wang<sup>1</sup>, Xing-Qiu Chen<sup>1,\*</sup>, Dianzhong Li<sup>1</sup>, Yiyi

Li<sup>1</sup>, Petr Lazar<sup>2,3</sup>, Raimund Podloucky<sup>2</sup>, and Aleksey N. Kolmogorov<sup>4</sup>

<sup>1</sup> *Shenyang National Laboratory for Materials Science, Institute of Metal Research, Chinese Academy of Sciences, Shenyang 110016, China*

<sup>2</sup> *Center for Computational Materials Science, University of Vienna, Sensengasse 8, A-1090 Vienna, Austria*

<sup>3</sup> *Regional Centre of Advanced Technologies and Materials, Department of Physical Chemistry, Faculty of Science, Palacky University Olomouc, Tr. 17. Listopadu 12, 771 46 Olomouc, Czech Republic and*

<sup>4</sup> *Department of Materials, University of Oxford, Parks Road, Oxford OX1 3PH, United Kingdom*

(Dated: March 1, 2013)

By electron and X-ray diffraction we establish that the CrB<sub>4</sub> compound discovered over 50 years ago crystallizes in the *oP10* (*Pnmm*) structure, in disagreement with previous experiments but in agreement with a recent first-principles prediction. The 3D boron network in the new structure is a distorted version of the rigid carbon *sp*<sup>3</sup> network proposed recently for the high-pressure C<sub>4</sub> allotrope. According to our density functional theory calculations and the analysis of the bonding, CrB<sub>4</sub> is a potentially superhard material. In fact, the calculated weakest shear and tensile stresses exceed 50 GPa and its Vickers hardness is estimated to be 48 GPa.

PACS numbers: 62.40.+i, 62.20.Qp, 71.20.Be, 63.20.dk

Covalent networks with high atomic densities and three-dimensional (3D) morphologies [1–5] are basic features of most of the known superhard materials, including diamond [Fig. 1(a)], *c*-BC<sub>2</sub>N, *c*-BN, and the recently found compounds *c*-BC<sub>5</sub> [6] and  $\gamma$ -B<sub>28</sub> [7–9]. Three new promising superhard allotropes of carbon with strong quasi-*sp*<sup>3</sup> covalent bonding as realized in a monoclinic (M-carbon[10]), tetragonal body-centered (bct-C<sub>4</sub> [11, 12]), and orthorhombic (W-carbon [13]) structure have been proposed for the interpretation of the X-ray diffraction pattern of cold-compressed graphite[14]. In particular, metastable bct-C<sub>4</sub> is built up by an unusual framework [15] of interconnected square C<sub>4</sub> units [Fig. 1(b)] and has been predicted to be superhard by several first-principles studies [16–19]. Inspired by the search for superhard materials which can be fabricated without the need of an expensive high pressure [20] or a chemical vapor deposition [21] methods, we re-examine a known stable intermetallic CrB<sub>4</sub> compound comprised of similar B<sub>4</sub> units. We find that, compared to the ReB<sub>2</sub> compound shown recently to have a remarkably high hardness [20, 22–24], CrB<sub>4</sub> holds the promise to have even more outstanding mechanical properties.

First we characterize CrB<sub>4</sub> experimentally by means of electron diffraction (ED) and X-ray diffraction (XRD) techniques confirming a first-principles prediction [25, 26] that the orthorhombic structure of CrB<sub>4</sub>, originally suggested to have the *Immm* space group (with the *oI10* unit cell in Pearson notation, see Fig. 1(c)), has a lower-symmetry *Pnmm* space group (*oP10*, see Fig. 1(d)). On the basis of density functional theory (DFT) calculations [27–30], we establish that CrB<sub>4</sub> with the newly claimed structure has lowest ideal tensile and shear strengths of 51 GPa, which are comparable to those of cubic boron

nitride (*c*-BN). Making use of an empirical model [31, 32] correlating the elastic moduli and Vickers hardness ( $H_v$ ), we estimate  $H_v \approx 48$  GPa, which exceeds significantly the 40 GPa threshold of superhardness. To rationalize this finding we perform a DFT study of the ten transition metal borides, *TMB*<sub>4</sub> (with *TM* = Ti, V, Cr, Mn, Fe as well as *TM* = Zr, Nb, Mo, Tc, Ru). Our results indicate that the atomic size and valence of the *TM* elements play a key role in determining the mechanical properties. The hardness reaches a maximum for *TM*=Cr when all bonding B quasi-*sp*<sup>3</sup> and hybridized Cr-B states become occupied.

In 1968, Andersson and Lundström [33] reported the synthesis of CrB<sub>4</sub> and characterized it as an orthorhombic *oI10* structure. Given the very good fit of the X-ray pattern to the *oI10* structure and the recently demonstrated elastic stability of the compound[34] there was no reason to suspect incompleteness of this structural model. However, examination of the ground states of

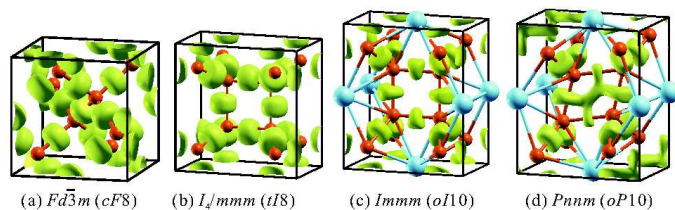


FIG. 1: (color online) Isosurfaces of the electron localization function (ELF) [35], corresponding to a value of 0.75. (a,b): diamond and bct-C<sub>4</sub> carbon; (c,d): orthorhombic structures of CrB<sub>4</sub>. Small and large balls denote B and Cr atoms, respectively.

Fe-B [25] and Cr-B systems [26] revealed a dynamical instability of the  $oI10$  structure due to phonon modes with imaginary frequency near  $\mathbf{q} = \mathbf{0}$ . As a consequence, the boron framework undergoes a significant distortion transforming the orthorhombic body-centered structure ( $oI10$ ) into a primitive one ( $oP10$ ). It was observed [26] that this structural transformation leaves the unit cell dimensions and the XRD patterns essentially unchanged (see Fig. S2 in Ref. [36]) which necessitates the use of an alternative characterization technique to finally resolve the structure of  $\text{CrB}_4$ .

A 20g sample with the initial composition of  $\text{CrB}_4$  was prepared by repeated arc-melting of electrolytic chromium (from Alfa Aesar, claimed purity 99.997%) and crystalline boron pieces (from Alfa Aesar, claimed purity 99.5%) under argon atmosphere. Cut sample pieces were sealed in quartz under argon and annealed in a high temperature furnace for 192 hours at 1250 °C. The annealed samples were characterized via metallographic microscope (LEISS Axiovert 200 MAT), scanning electron microscope (SEM, HITACHI S-3400N) in the back-scattered electron mode (BSE). Our electron probe microanalyser (EPMA, SHIMADZU EPMA-1610) results showed 20.374 at.% and 79.626 at.% elemental compositions of Cr and B, respectively. The presence, distribution, and phase characteristics of  $\text{CrB}_4$  (78.06%),  $\text{CrB}_2$  (7.32%), and amorphous boron (14.62%) were further analyzed with an electron backscatter diffraction (EBSD) micrograph [36]. TEM characterization of finely ground samples [36] was carried out with Tecnai G2 F20 S-TWIN transmission electron microscope. Finally, we obtained X-ray diffraction (XRD) patterns using a Rigaku diffractometer and  $\text{Cu } K_\alpha$  irradiation ( $\lambda=1.54056 \text{ \AA}$ ) and performed full Rietveld refinement using the FULLPROF package [37].

For DFT calculations we used the Perdew-Burke-Ernzerhof exchange-correlation functional [27] within the generalized gradient approximation and the projector-augmented waves method [28] as implemented in VASP [29, 30]. The energy cutoff was set at 500 eV. We allowed spin polarization for all  $\text{TM}_4\text{B}_4$  but only one compound of  $\text{MnB}_4$  showed a small non-zero magnetic moment of about  $0.7 \mu_B$  per Mn in the antiferromagnetic ordering. A very accurate optimization of structural parameters was achieved by minimizing forces (below 0.001 eV/Å) and stress tensors (typically below 0.5 kBar). Further simulation details and the procedure for calculating the mechanical properties are described in the supplementary material [36].

Figure 2 shows our experimental ED patterns projected along the [100], [110], [111] and [101] directions revealing that the unit cell has the dimensions  $|a^*| \approx 2.1 \text{ nm}^{-1}$ ,  $|b^*| \approx 1.8 \text{ nm}^{-1}$ ,  $|c^*| \approx 3.5 \text{ nm}^{-1}$  and it can be classified as a primitive orthorhombic lattice. The simulated ED pattern along [101] for the  $oP10$  structure (Fig. 2f) shows additional reflections as compared to  $oI10$  (Fig.

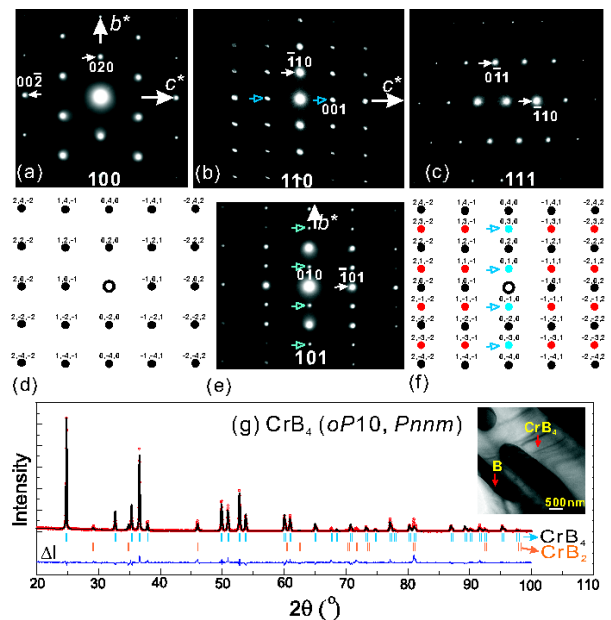


FIG. 2: (color online) (a-c,e) Experimental electron diffraction (ED) patterns along the [100], [110], [111] and [101] directions, respectively. (d,f): theoretical [101] ED patterns for  $oI10$  and  $oP10$  structures, respectively; (g) Rietveld refinement ( $\text{Cu } K_{\alpha 1}$ ) of the experimental X-ray diffraction data; reflections of  $\text{CrB}_2$  are indicated by vertical bars. Hollow arrows in (b,e,f) denote the second-order diffraction spots. Inset in (g) is a TEM image showing the phase boundary of  $\text{CrB}_4$ .

2d), which is expected because the unit cell is doubled and the number of symmetry operations is reduced from 16 to 8. The corresponding extra reflections are clearly present in the observed [101] pattern which unambiguously points at the  $oP10$  structure. The  $oP10$  structural model was further used to refine the powder XRD data and by that a good agreement between experiment and theory is obtained (see Table S1 in Ref. [36]).

The mechanism causing the observed distortion in  $\text{CrB}_4$  is many fold, because it is related to the quasi- $sp^3$  B-B bonding, the hybridization of the B- and Cr-like states, the atomic size of Cr relative to the available volume in the B cage and the charge transfer between B and Cr (i.e. the valencies). It is illustrative to look first at the evolution of the B network in the sequence of the related structure types: diamond,  $\text{bct-C}_4$ ,  $oI10$ , and  $oP10$  (see Fig. 1). In diamond, the tetrahedral arrangement of four nearest neighbors with the  $\cos^{-1}(-1/3) \approx 109.5^\circ$  angles between the bonds is optimal for the  $sp^3$  hybridization [38] (Fig. 1(a)). In  $\text{bct-C}_4$ , the symmetry of the local atomic environment is broken as two bonds form a  $90^\circ$  angle (Fig. 1(b)). In  $oI10$ , symmetry is further reduced due to the two bonds now having different lengths (namely, 1.73 Å and 1.86 Å for structurally relaxed  $\text{CrB}_4$ , see Fig. 1(c)). Finally, in  $oP10$  a further deviation from the ideal  $sp^3$  geometry

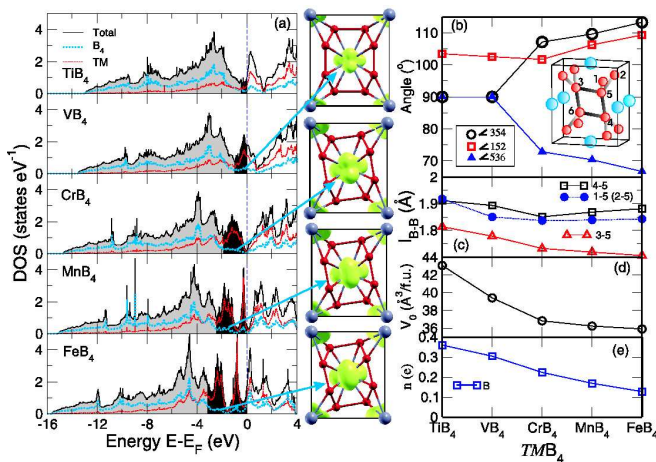


FIG. 3: (color online) Calculated electronic structure of TMB<sub>4</sub> compounds (TM: 3d transition elements). (a): electronic densities of states (DOS) with occupied bonding and nonbonding states highlighted in grey and black, respectively. The corresponding insets of structures show charge density isosurfaces (0.1 e/Å<sup>3</sup>) for the energy windows corresponding to the nonbonding states. (b-e): variation of bond angles, bond lengths, atomic volume, and charge transfer to boron obtain by Bader’s decomposition.[40]

occurs as one of the two nonequivalent B sites has two B-B bonds at an angle well below 90° and the other is no longer four-fold coordinated (a fifth B atom is 2.13 Å away and the electron localization function shown in Fig. 1(d) develops a blob along the short diagonal of the B parallelogram).

Within a semiempirical extended Hückel approach Burdett *et al.* [39] studied the relative stability of carbon- and boron-based structures by analyzing the moments ( $\mu_n$ ) of the electronic density of states (DOS). They argued, that bct-C<sub>4</sub>-carbon is less stable than diamond-carbon because (i) the non-optimal 90° angle gives rise to a strain energy and (ii) the four-membered rings result in a higher  $\mu_4$  which translates into a more unimodal DOS and a lower stability for elements with a half-filled shell. Their conclusion that the second contribution could stabilize boron-based materials with a lower number of electrons is supported by our DFT calculations: for the group-IV carbon the diamond structure is favored by 0.20 eV/atom while for the group-III boron the bct-C<sub>4</sub> structure is favored by 0.08 eV/atom. The structural differences within the bct-C<sub>4</sub>, *oP10*, and *oP10* family are less pronounced. However, the presence of three-membered rings in *oP10* may significantly influence the structure’s important third and fourth DOS moments.

To elucidate the stabilization role of the TM atom we carried out a series of DFT calculations for ten TMB<sub>4</sub> compounds. The DOS and formation enthalpies are presented for the more stable of the *oI10* or *oP10* structure. For the 3d series Fig. 3(a) shows rather similar DOS

profiles with the Fermi level ( $E_F$ ) moving upwards as the electron count increases. In the exemplary CrB<sub>4</sub> case, the DOS in the range of (-14, -5) eV is mostly of B-s - p-like character. The weight of the Cr DOS increases gradually and in the range of (-5, -2) eV a strong hybridization between Cr- $d_{xy}$  ( $-d_{xz}$ ) and B- $p_y$  ( $-p_z$ ) states is observed. In the region from -2 to 0 eV the Cr- $d_{(x^2-y^2)}$  and Cr- $d_{yz}$  nonbonding states become dominant. The position of  $E_F$  in the pseudogap along with the lowest formation enthalpy achieved for TM = Cr (see Fig. 4c) is consistent with the prediction[39] of maximum stability occurring in the middle of the 3d series. Further DFT calculations as detailed in the supplementary material [36] shed light on the stability competition between the *oP10* and the *oI10* structures. We find that Ti and V as well as Zr, Nb, and Mo tetraborides prefer the *oI10* type. Furthermore, the energy gained by the *oI10* to *oP10* transformation is larger for the 3d compounds and increases within both series from left to right. It is also noticeable, that the structural transformation is accompanied by a volume reduction whereby over 80% of the energy gain comes just from the distortion of the B network. Finally, by artificially decreasing (increasing) the volume one can induce (disfavor) the distortion for all the considered TMB<sub>4</sub> compounds. Figure 3(b-e) summarizes the structural trends and shows the variation of the average Bader’s charge [40]. We employ the Bader’s charge decomposition to illustrate that the charge transfer from the TM element to B (which is around 1 e/TM) decreases in the sequence from Ti to Fe. Hence, the distortion could be explained by the decreasing number of electrons transferred to B. The derived geometrical result, that three out of four B-B bonds have a minimum bond length for TM = Cr (Fig. 3c) demonstrates further why CrB<sub>4</sub> is particularly stable. Considering that  $E_F$  in FeB<sub>4</sub> moves from a deep valley in *oI10* into the shoulder of the antibonding B- $p$ -Fe- $d$  peak in *oP10* [25], the optimality of the  $p$ - $d$  bonding appears to be of less importance for the compound’s stability (note that the unexpectedly high DOS at  $E_F$  in *oP10*-FeB<sub>4</sub> makes the compound a good candidate to be a *phonon-mediated* superconductor with a  $T_c$  of 15-20 K [25]).

The mechanical properties of CrB<sub>4</sub> are examined and rationalized via DFT calculation of the elastic properties for the mentioned ten TMB<sub>4</sub> compounds (see Ref. [36]). All of them are found to exhibit ultra incompressibility along the  $b$ -axis and high bulk ( $B$ ) and shear ( $G$ ) moduli. CrB<sub>4</sub> is found to have the highest shear modulus ( $G = 261$  GPa) and Pugh’s ratio [41] ( $k = G/B = 261/265 = 0.985$ ), which are two important elastic properties thought to be strongly correlated to hardness [31]. The compound’s low Poisson ratio of  $\nu = 0.12$  is typical for materials with strong covalent bonding. [20] Strikingly, the calculated lowest ideal shear and tensile strengths of 51 GPa are remarkably high and comparable to the lowest tensile strength of 55 GPa for super-



TABLE I: Calculated elastic properties (in GPa) for CrB<sub>4</sub> and known (super)hard materials. The calculated bulk ( $B$ ) and shear moduli ( $G$ ) are Reuss-Voigt-Hill averages. The Vickers hardness estimates ( $H_v^{Calc}$ ) were obtained with our proposed formula [31, 32] using the calculated elastic moduli. Finally, the experimental Vickers hardness values ( $H_v^{Exp}$ ) for diamond, BC<sub>2</sub>N, bct-C<sub>4</sub>, c-BN and B<sub>4</sub>C were taken from Refs. [31, 45, 47]. Additional information is given in Table S5 [36].

	$C_{11}$	$C_{22}$	$C_{33}$	$C_{44}$	$C_{55}$	$C_{66}$	$C_{12}$	$C_{13}$	$C_{23}$	$B$	$G$	$H_v^{Calc}$	$H_v^{Exp}$
Diamond	1079			578			124			442	536	95.7	96±5
BC <sub>2</sub> N										408	445	75.4	76±2
bct-C <sub>4</sub>	933		1190	447		325	172	59		404	421	68.9	
c-BN	820			480			190			400	405	65.2	66±2
B <sub>4</sub> C										247	200	31.7	30±2, 31.3-38.9, 42-49
CrB <sub>4</sub> ( <i>oP</i> 10)	554	880	473	254	282	250	65	107	95	265	261	48.0	
CrB <sub>4</sub> ( <i>oI</i> 10)	591	931	467	252	280	225	64	115	97	275	259	45.1	

hard *c*-BN [42]. These values exceed considerably the lowest ideal shear strength of 34 GPa [42] in ReB<sub>2</sub> which structure is comprised of buckled 2D boron nets[43]. As a corroboration for a possibly outstanding hardness, by breaking Cr-B bonds along the [001] direction we found the lowest critical cleavage stress [44] of 53 GPa, which matches the lowest ideal strengths. Finally, for estimation of the Vickers hardness ( $H_v$ ) in terms of elastic properties we employ a recently proposed empirical model[31, 32],  $H_v = 2.0(k^2G)^{0.585} - 3.0$  ( $H_v$  and  $G$  in GPa), which performs well across a large class of materials and hardness values (Fig. 4, panel (a)). Figure 4 reveals that the predicted behavior of  $H_v$  for the TMB<sub>4</sub> compounds (panel b) mirrors the trend in their enthalpy of formation (panel c). The largest hardness value of

$H_v = 48$  GPa for CrB<sub>4</sub> is well above the superhardness threshold of 40 GPa and decreases rapidly for the considered TMs. In particular, the isoelectronic but larger Mo atom stretches the B network beyond its optimal size, leading to a 25% reduction in hardness. When compared against the known B<sub>4</sub>C material which can also be synthesized under ambient pressure, CrB<sub>4</sub> displays (see Table I) superior elastic properties and estimated  $H_v$  (note that according to recent measurements B<sub>4</sub>C is not superhard in its crystalline form [45]).

Our findings make *oP*10-CrB<sub>4</sub> a prime candidate to be an (up-to-now overlooked) affordable ambient-pressure superhard material. Measurement of the compound's Vickers hardness will be a challenge as pure CrB<sub>4</sub> samples are difficult to produce with standard methods due to the particular behaviour of the Cr-B system in the high-temperature - B-rich part of the binary phase diagram [46]. Namely, the cooling of an arc-melted 1:4 elemental mixture leads unavoidably to a two-phase coexistence of CrB<sub>2</sub> and B in a wide high-temperature region from 1830 °C to 1500 °C. Formation of CrB<sub>4</sub> occurs below 1500 °C but significant fractions of CrB<sub>2</sub> and B can still be present after week(s) of sample annealing, as happened in the original [33] and present [36] studies. Our currently best samples with 78% content of CrB<sub>4</sub> allowed us to reliably characterize the compound's crystal structure but were not suitable for investigation of its mechanical properties. Therefore, alternative approaches, such as the powder metallurgical process or the single-crystal growth method, may need to be employed to obtain samples of desired quality.

The confirmation of the new *oP*10 crystal structure of CrB<sub>4</sub> makes the prospect of synthesizing the FeB<sub>4</sub> phase with the same structure -predicted to be a viable high-temperature and high-pressure ground state of the Fe-B system [25, 26]- more exciting. Our detailed experimental and theoretical study of the presumably superhard compound CrB<sub>4</sub> demonstrates that materials with appealing properties may still be found in reportedly well-known binary systems.

**Acknowledgement** We thank Xiaobing Hu and Prof. Shaobo Mi in the IMR for their valuable helps in per-

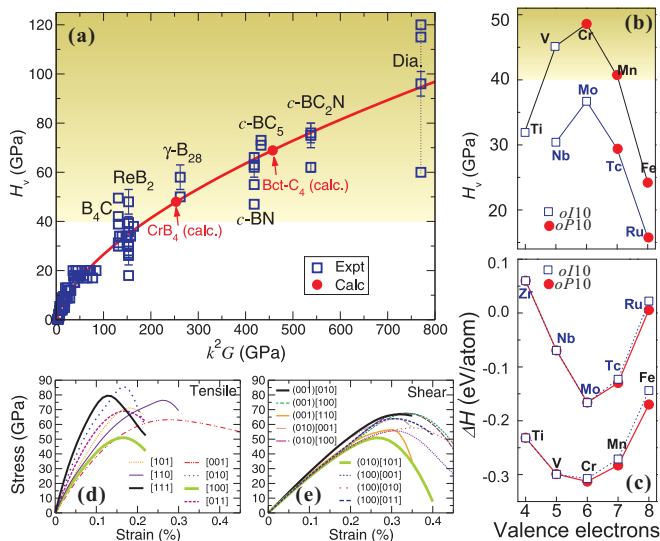


FIG. 4: (color online) (a): Vickers hardness,  $H_v$ , as a function of  $k^2G$ , with  $k$  being the ratio of the shear ( $G$ ) to bulk ( $B$ ) modulus; the experimental data are discussed in the supplementary material [36]; (b):  $H_v$  for the most stable TMB<sub>4</sub> structures derived from the calculated  $B$  and  $G$  values (see text and Ref. 31); (c): formation enthalpy; (d,e): ideal tensile and shear strengths of *oP*10-CrB<sub>4</sub>.

forming and analyzing ED experiments and Prof. Shi Liu for his help in synthesizing experimental samples. We are grateful for supports from the “Hundred Talents Project” of Chinese Academy of Sciences and from NSFC of China (Grand Numbers: 51074151, 51174188) as well as Beijing Supercomputing Center of CAS (including its Shenyang branch in the IMR). A.N.K acknowledges the support from EPSRC CAF EP/G004072/1 in the UK.

---

\* Corresponding author: xingqiu.chen@imr.ac.cn

- [1] R.B. Kaner, J.J. Gilman, and S.H. Tolbert, *Science*, **208**, 1268 (2005).
- [2] V. V. Brazhkin, A. G. Lyapin, and R. J. Hemley, *Philos. Mag. A*, **82**, 231 (2002).
- [3] V. V. Brazhkin, N. Dubrovinskaia, M. Nicol, N. Novikov, R. Riedel, V. Solozhenko, and Y. Zhao, *Nat Mater*, **3**, 576 (2004).
- [4] J. J. Gilman. *Science* **261**, 143 (1993).
- [5] S. Veprek, *J. Nanosci. Nanotechnol.*, **11**, 14 (2011).
- [6] V. L. Solozhenko, O. O. Kurakevych, D. Andrault, Y. L. Godec, and M. Mezouar, *Phys. Rev. Lett.*, **102**, 015506 (2009).
- [7] V. L. Solozhenko, O. O. Kurakevych and A. R. Oganov, *J. Superhard Mater.*, **30**, 428 (2008).
- [8] A. R. Oganov, J. H. Chen, C. Gatti, Y. Z. Ma, Y. M. Ma, C. W. Glass, Z. X. Liu, T. Yu, O. O. Kurakevych, and V. L. Solozhenko, *Nature*, **457**, 863 (2009).
- [9] E. Y. Zarechnaya, L. Dubrovinsky, N. Dubrovinskaia, Y. Filinchuk, D. Chernyshov, V. Dmitriev, N. Miyajima, A. El Goresy, H. F. Braun, S. Van Smaalen, I. Kantor, A. Kantor, V. Prakapenka, M. Hanfland, A. S. Mikhaylushkin, I. A. Abrikosov, and S. I. Simak, *Phys. Rev. Lett.*, **102**, 185501 (2009).
- [10] Q. Li, Y. Ma, A. R. Oganov, H. Wang, H. Wang, Y. Xu, T. Cui, H. K. Mao, and G. Zou, *Phys. Rev. Lett.* **102**, 175506 (2009).
- [11] K. Umemoto, R. M. Wentzcovitch, S. Saito, and T. Miyake, *Phys. Rev. Lett.* **104**, 125504 (2010).
- [12] R. H. Baughman and D. S. Galvao, *Phys. Rev. Lett.* **104**, 125504 (2010).
- [13] J.-T. Wang, C. Chen, and Y. Kawazoe, *Phys. Rev. Lett.* **106**, 075501 (2011).
- [14] W.L. Mao, H.-k. Mao, P. J. Eng, T.P. Trainor, M. Newville, C.-c. Kao, D. L. Heinz, J. F. Shu, Y. Meng and R. J. Hemley, *Science*, **302**, 425 (2003).
- [15] H. Y. Niu, X.-Q. Chen, S. B. Wang, D. Z. Li, W. L. Mao, Y. Y. Li, *Phys. Rev. Lett.*, **108**, 135501 (2012).
- [16] P. Y. Wei, Y. Sun, X.-Q. Chen, D. Z. Li, and Y. Y. Li, *Appl. Phys. Lett.*, **97**, 061910 (2010).
- [17] F.M. Gao and X.F. Hao, *Phys. Stat. Sol. (RRL) - Rapid Res. Let.*, **4**, 200 (2010).
- [18] H.Y. Niu, P.Y. Wei, Y. Sun, X.-Q. Chen, C. Franchini., D.Z. Li, and Y.Y. Li, *Appl. Phys. Lett.*, **99**, 031901 (2011).
- [19] Q. Zhu, A. R. Oganov, M. A. Salvadó, P. Pertierra, and A. O. Lyakhov, *Phys. Rev. B*, **83**, 193410 (2011).
- [20] J. B. Levine, S. H. Tolbert, and R. B. Kaner, *Adv. Funct. Mater.*, **19**, 3519 (2009).
- [21] P. F. Mcmillan, *Nat. Mat.*, **1**, 19 (2002).
- [22] J.B. Levine, J.B. Betts, J.D. Garrett, S.Q. Guo, J.T. Eng, A. Migliori, and R.B. Kaner, *Acta Mater*, **58**, 1530 (2010).
- [23] H.-Y. Chung, M.B. Weinberger, J.B. Levine, A. Kavner, J.-M. Yang and S.H. Tolbert, *Science* **316**, 436 (2007).
- [24] J.B. Levine, S.L. Nguyen, H.I. Rasool, J.A. Wright, S.E. Brown and R.B. Kaner, *J. Am. Chem. Soc.* **130**, 16953 (2008).
- [25] A. N. Kolmogorov, S. Shah, E. R. Margine, A. F. Bialon, T. Hammerschmidt, and R. Drautz, *Phys. Rev. Lett.*, **105**, 217003 (2010).
- [26] A. F. Bialon, T. Hammerschmidt, R. Drautz, S. Shah, E. R. Margine, and A. N. Kolmogorov, *Appl. Phys. Lett.*, **98**, 081901 (2011).
- [27] J.P. Perdew, K. Burke, and M. Ernzerhof, *Phys. Rev. Lett.* **77**, 3865 (1996).
- [28] P. E. Blöchl, *Phys. Rev. B*, **50**, 17953 (1994).
- [29] G. Kresse and J. Hafner, *Phys. Rev. B* **47**, 558 (1993).
- [30] G. Kresse and J. Furthmüller, *Phys. Rev. B* **54**, 11169 (1996).
- [31] X.-Q. Chen, H. Y. Niu, D. Z. Li and Y. Y. Li, *Intermetallics*, **19**, 1275 (2011).
- [32] X.-Q. Chen, H. Y. Niu, C. Franchini, D. Z. Li and Y. Y. Li, *Phys. Rev. B*, **84**, 121405(R) (2011).
- [33] S. Andersson, and T. Lundström, *Acta Chem. Scand.*, **22**, 3103 (1968).
- [34] H. B. Xu, Y. X. Wang and V. C. Lo, *Phys. Stat. Sol. (RRL) - Rapid Res. Let.*, **5**, 13 (2011).
- [35] B. Silvi and A. Savin, *Nature (London)*, **371**, 683 (1994).
- [36] See supplementary material at <http://link.aps.org/supplementary/>.
- [37] J. Rodriuez-Carvajal, *Physica B*, **192**, 55 (1993).
- [38] D. G. Pettifor, *Bonding and Structure of Molecules and Solids*, (Clarendon Press) 1995.
- [39] J. K. Burdett and S. Lee, *J. Am. Chem. Soc.* **107**, 3063 (1985).
- [40] W. Tang, E. Sanville and G. Henkelman, *J. Phys.: Condens. Matter* **21**, 084204 (2009).
- [41] S. F. Pugh, *Philos. Mag. Ser. 7*, **45**, 823 (1954).
- [42] R. F. Zhang, S. Veprek, and A. S. Argon, *Appl. Phys. Lett.*, **91**, 201914 (2007).
- [43] X.-Q. Chen, C. L. Fu, M. Krčmar, and G. S. Painter, *Phys. Rev. Lett.*, **100**, 196403 (2008).
- [44] P. Lazar and R. Podloucky, *Phys. Rev. B*, **78**, 104114 (2008).
- [45] S. Grasso, C. Hu, O. Vasyukiv, T. S. Suzuki, S. Guo, T. Nishimura and Y. Sakka, *Scripta Materialia*, **64**, 256 (2011).
- [46] T. B. Massalski and H. Okamoto, *Binary Alloy Phase Diagrams*, (ASM Intl; 2nd ed., ASM International 1990).
- [47] P. S. Kislyi, *Superhard and Refractory Materials*, (Kiev: Institute of Superhard Materials), p.86, 1985